Analysis of the Electromagnetic Waves in an Overmoded Finite Length Slow Wave Structure

Md. Ruhul Amin, K. Ogura, H. Kitamura, K. Minami, T. Watanabe, Y. Carmel, *Senior Member, IEEE*, W. Main, J. Weaver, W. W. Destler, *Fellow, IEEE*, and V. L. Granatstein, *Fellow, IEEE*

***Abstract*—The electromagnetic fields of the higher order axial resonant modes in a slow wave structure are analyzed and found to have considerably different characteristics from those of the conventional fundamental mode. Here, the reflections at both ends produce axial resonant modes corresponding to axisymmetric transverse magnetic (TM) modes. The period of field modulation of some of the higher order axial modes is shorter than that of the usual mode in a cylindrical waveguide, which could be of practical interest for higher power, higher frequency operation of backward wave oscillators. A perturbation technique is used to ascertain the field distribution inside the resonant cavity, and the numerical results thus obtained are compared to some experimental data.**

I. Introduction

THE growing need for coherent, efficient, and high power microwaves has led to the development of a number of innovative devices, including backward wave oscillators (BWO's), which are a promising class of devices having a number of useful features, namely: high spectral purity microwave power, frequency tunability, high efficiency, etc. [1]–[5]. For example, for an overmoded structure, $D/\lambda > 1$. 7% frequency tunability in the frequency range 5.2–5.6 GHz has been reported [6]. Here, D is the mean diameter of the waveguide and λ is the wavelength. Microwave radiations on the order of 1 GW at a frequency up to 30 GHz have been obtained [7], [8]. Continuous efforts are being made to enhance the power and frequency level of the devices.

In the slow wave devices, the interaction of electromagnetic (EM) quantities takes place inside the slow wave structures (SWS). In order to understand the physics of the mechanism involved, it is necessary to analyze the SWS in a realistic way. Resonators are also used in linear accelerator (linac), but their geometries are considerably different from those used in BWO's. The EM behaviors of the linac cavities have been extensively studied by many researchers using numerical computational techniques. In order to study the accelerator cavities with complex geometries, computational codes such as SUPERFISH [9], URMEL-T [10], etc., have been developed. These codes are based on the discretization techniques of Maxwell's and Helmholtz's equation, in general. The computational time of these codes depends on the number of mesh points, geometry of the cavity, boundary conditions, and accuracy demanded for the particular purpose. A brief description of the numerical codes generally used in linac studies is presented in [11] by Cooper and Jones. In this work, an attempt has been made to explore the EM quantities of a sinusoidally corrugated SWS typically used in the BWO experiments in the simplest way, by using analytic equations derived for this purpose. In the BWO's, the finite axial dimension of the SWS causes reflections from the ends and, thereby, quantization of the axial wavenumber results in axial resonant modes. The finite transverse dimension of the SWS limits the power handling capability due to the internal RF breakdown. In order to overcome such a problem, one can increase the mean diameter of the SWS, thus creating an overmoded system. In general, many higher modes can be oscillated in such an overmoded SWS. It is still possible to operate the BWO preferentially at a particular mode with higher frequency by carefully selecting the beam and size parameters. This is because the respective modes have different starting current for oscillation with each other. This difference can be carefully used to select the particular mode for oscillation. In fact, recent experiments have shown that efficient and high power output can be achieved in such devices operating in a single mode [6]. Despite the numerous studies on conventional, weakly relativistic microwave tubes, more detailed studies of the resonant modes in the finite length SWS's intended for operation with highly relativistic electron beams are required. The motivation of the present work is the recent interest in the generation of high power microwave radiation employing overmoded slow wave systems. Most of the analyses of such systems were performed assuming infinite length systems or perfectly matched finite length systems, which are far from the actual experiments. Moreover, their analyses have been restricted mainly to the fundamental mode [12]–[18]. In this paper, we model a finite length SWS consistent with real experiments and include higher order modes in our computations. Specifically, we consider the two wave interaction process with 100% round-trip reflection. Under this assumption, our SWS becomes an SWS cavity with perfectly shorted ends. Detailed field calculations along with higher harmonic analysis of the axial resonant modes in the SWS have been made. For the higher order axisymmetric TM modes ($TM_{0s}, s > 1$), some unusual and novel phenomena

Manuscript received March 11, 1994; revised August 4, 1994.

M. R. Amin, K. Ogura, H. Kitamura, and K. Minami are with the Graduate School of Science and Technology, Niigata University, Niigata City, 950-21, Japan.

T. Watanabe is with the National Institute for Fusion Science, Nagoya, 464-01, Japan.

Y. Carmel, J. Weaver, W. W. Destler, and V. L. Granatstein are with the Institute for Plasma Research, University of Maryland, College Park, MD 20742 USA.

W. Main is with ACCURAY Inc., Santa Clara, CA USA.

IEEE Log Number 9408564.

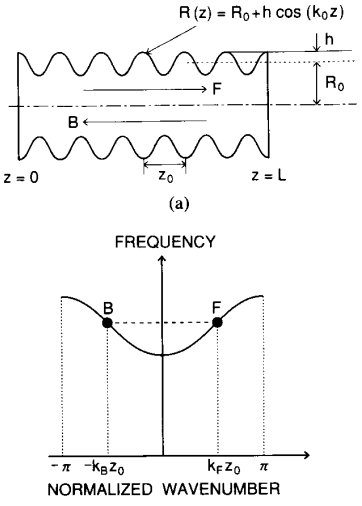

Fig. 1. Schematic diagram of a spatially periodic slow wave structure (SWS) showing the directions of forwardly propagating wave F and backwardly propagating wave B. (a) SWS shorted at $z = 0$ and $z = L$ and (b) locations of the F and B waves in the dispersion curve in the first Brillouin zone.

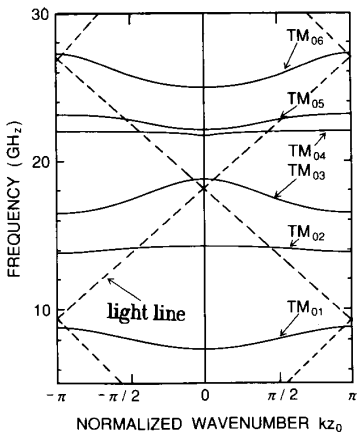

Fig. 2. Numerically obtained dispersion relations of the SWS for $-\pi \leq kz_0 \leq \pi$ in the first Brillouin zone. The parameters of the SWS are: $R_0 = 1.4499$ cm, $z_0 = 1.67$ cm, and $h = 0.406$ cm. Light lines ($\omega/k = c$) are shown by dashed lines.

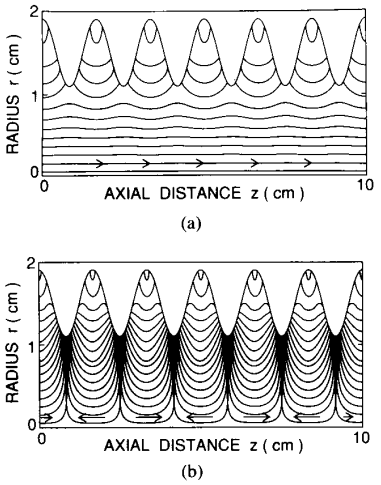

Fig. 3. Electric field patterns of the TM_{01} mode. SWS parameters are: $R_0 = 1.499$ cm, $z_0 = 1.67$ cm, and $h = 0.406$ cm. Arrows indicate the direction of the electric field. The density of the field lines indicates the strength of electric field qualitatively. (a) $TM_{01}(0\pi/6)$ mode and (b) $TM_{01}(6\pi/6)$ mode.

have been found for the first time regarding the amplitude of the spatial harmonic components of the resonant modes for particular values of the axial wavenumber. Cavity perturbation technique [19] has been employed to calculate the resonant frequency shift of the cavity. Some of the present numerical results are compared to experimental and numerical results obtained by using SUPERFISH in [20], and are found to be in excellent agreement.

The organization of the paper is as follows. In Section II, we present the mathematical formulation of the SWS. Section III describes the numerical results of the analysis. The cavity perturbation technique and the corresponding numerical and experimental results are given in Section IV. In Section V, discussion and conclusion of the present works are presented.

II. Mathematical Formulation

First, we consider an infinite length SWS; next, after imposing additional axial boundary condition to the system, we will obtain the EM field quantities in a finite length SWS. As depicted in Fig. 1(a), the SWS is assumed to be sinusoidally corrugated in the axial direction with radius $R(z) = R_0 + h\cos k_0 z$, where $k_0 = 2\pi/z_0$. Physical quantities associated with an EM mode are represented by a spatial harmonic series satisfying Floquet's theorem. For axisymmetric TM modes, the axial electric field E_z can be expressed as [14], [16]

$$E_z(z, r, t) = \sum_{n=-\infty}^{\infty} A_n J_0\left(\frac{x_n}{R_0} r\right) e^{i(k_n z - \omega t)} \qquad (1)$$

where J_0 is the 0th-order Bessel's function of the first kind, $x_n^2 = R_0^2(\omega^2/c^2 - k_n^2)$, $k_n = k + nk_0$, k is the axial wavenumber, and n is an integer. For slow spatial harmonic waves with $x_n^2 < 0$, Bessel's function J_0 becomes the modified Bessel's function I_0. Although the contributions of these harmonics are substantial inside the deep corrugation ($r \sim R_0 + h$), this region is so small that we can still determine the EM characteristics inside the SWS correctly. The other components, E_r and H_θ, are derived from E_z. The dispersion relation is obtained from the boundary condition at the wall of the structure, i.e., the tangential component of electric field should be zero at $r = R(z)$. The mth spatial Floquet harmonic components of this boundary condition can be expressed as

$$\sum_{n=-\infty}^{n=\infty} A_n \int_{-z_0/2}^{z_0/2} e^{i[(n-m)kz]} \left(1 + \frac{ik_n}{(\omega^2/c^2 - k_n^2)} \frac{\partial}{\partial z}\right) \cdot J_0\left(\frac{x_n}{R_0} R\right) dz = 0.$$

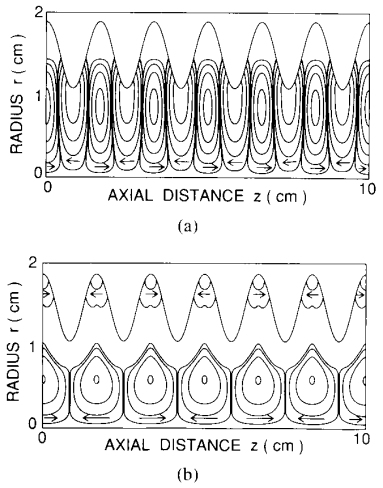

Fig. 4. Electric field patterns of the TM_{04} mode. SWS parameters are the same as in Fig. 3. Arrows indicate the direction of electric field. The density of the field lines indicates the strength of the electric field qualitatively. (a) $TM_{04}(0\pi/6)$ mode and (b) $TM_{04}(6\pi/6)$ mode.

In order to evaluate this integral, we used Taylor series expansion of the Bessel's function around $R = R_0$, since direct integration takes much time for computation. The radial boundary condition is imposed into the following matrix form:

$$[D] \cdot [A] = 0 \tag{2}$$

where $[A]$ is a column vector with elements A_n, and $[D]$ is a matrix of an infinite rank with each element given by $D_{mn} = [1 + (n - m)Q_n]C_{mn}$ where

$$C_{mn} = \sum_{q=0}^{\infty} \frac{(x_n \alpha)^{2q+|n-m|} J_0^{(2q+|n-m|)}(x_n)}{2^{2q+|n-m|} q!\,(q + |n - m|)!} \tag{3}$$

$Q_n = k_0 k_n/(\omega^2/c^2 - k_n^2)$ and $a = h/R_0$. The dispersion relation is determined from the condition that (2) should have nontrivial solutions, and is given by

$$D(k.\ \omega) = \det [D] = 0. \tag{4}$$

In our practical calculation, the value of n is limited to $-4 \leq n \leq 4$, and $2q + |n - m| \leq 10$ is chosen in (3). By comparing to direct integration, we have confirmed that the Taylor expansion of the Bessel's function converges quite rapidly and that the numerical errors are less than 1% for the fundamental mode with the parameters later described.

In the case of a finite length SWS, the additional boundary condition at both ends of the structure must be included. Referring to Fig. 1(a), a forward propagating wave F in the z-direction is reflected at $z = L$ and becomes a backwardly propagating wave B. The locations of the waves on the dispersion curve are shown in Fig. 1(b). Both F and B waves have to satisfy (4). The F wave propagates from the $z = 0$ boundary. After a round-trip with reflection at $z = L$, the resultant wave at the $z = 0$ boundary should be "single" valued. This is a two wave interaction process, and the axial boundary condition can be expressed as [16]

$$Re^{i(k_F - k_B)L} = 1 \tag{5}$$

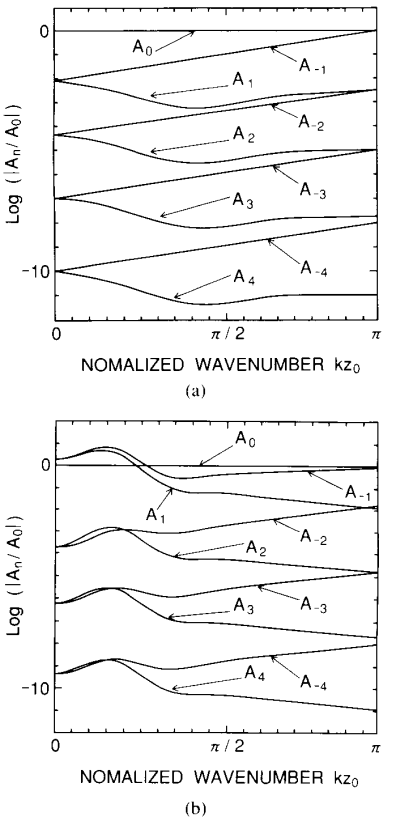

Fig. 5. Relative magnitude of the amplitude of the Floquet harmonics A_n versus normalized wavenumber for $0 \leq kz_0 \leq \pi$. (a) TM_{01} mode and (b) TM_{04} mode.

where R is the total reflection coefficient at the ends of the SWS, and k_F and k_B are the wavenumbers of the F and B waves, respectively. If the cavity is lossless and the ends are shorted with perfectly conducting metal plates, then $R = 1$ and $k_F = -k_B$ as shown in Fig. 1(b). Hence, from (5), $k_F = N\pi/L$, where N is an integer. Except for the propagating direction, the wave B is the same as the wave F. They satisfy identical radial boundary conditions and have the same energy. Therefore, in (1), the relationship between the coefficients A_n can be written as $A_n^F = A_{-n}^B$. By summing the F and B waves, the expressions of the EM fields in the SWS cavity become

$$E_z(z, r, t) = e^{-i\omega t} \sum_{n=-\infty}^{\infty} 2A_n J_0\left(\frac{x_n}{R_0} r\right) \cos(k_n z) \tag{6}$$

$$E_r(z, r, t) = R_0 e^{-i\omega t} \sum_{n=-\infty}^{\infty} \frac{2A_n k_n}{x_n} J_1\left(\frac{x_n}{R_0} r\right) \sin(k_n z) \tag{7}$$

$$H_\theta(z, r, t) = -i\epsilon_0 \omega R_0 e^{-i\omega t} \cdot \sum_{n=-\infty}^{\infty} \frac{2A_n}{x_n} J_1\left(\frac{x_n}{R_0} r\right) \cos(k_n z). \tag{8}$$

Once the dispersion relation (4) is solved numerically, the

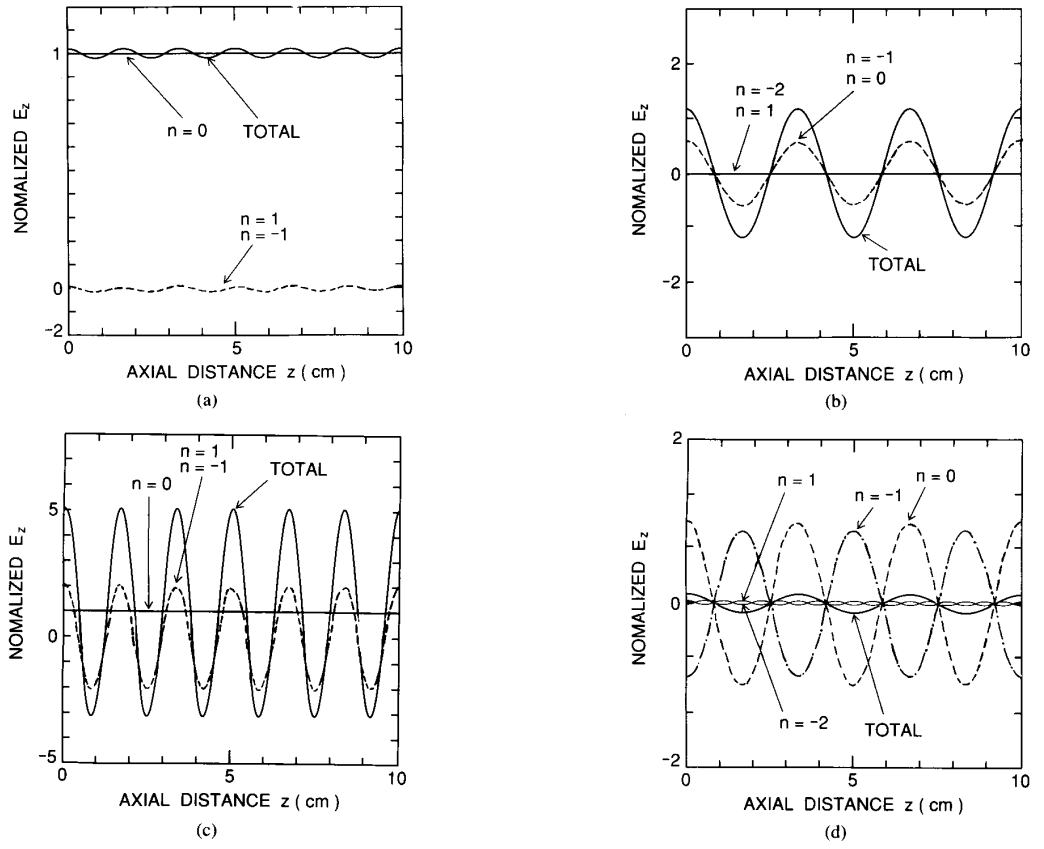

Fig. 6. Axial profiles of Floquet harmonics of field E_z at radial position $r = 0$ for TM_{01} and TM_{04} modes. The higher order harmonics of small amplitudes are not shown in the figures. Thick, solid curves represent the total value of the electric field E_z. Thin, dashed and chained curves represent the Floquet harmonics as indicated by n in the figures. (a) $TM_{01}(0\pi/6)$ mode, (b) $TM_{01}(6\pi/6)$ mode, (c) $TM_{04}(0\pi/6)$ mode, and (d) $TM_{04}(6\pi/6)$ mode.

relative magnitudes between the A_n factors are determined from (2). With a known set of values of A_n, the normalized values of the fields E_z, E_r, and H_θ can be calculated from (6), (7), and (8), respectively.

III. Numerical Results

In the present analysis, a six-period SWS having the following size parameters is considered: the mean radius $R_0 = 1.499$ cm; the period of corrugation $z_0 = 1.67$ cm; and the corrugation amplitude $h = 0.406$ cm. These dimensions correspond to the experimental values used by our research group at the University of Maryland [20]. Fig. 2 depicts dispersion relations computed from (4). The dashed lines in the figure are the light lines in free space. The end reflections cause the six-period SWS to resonate at seven distinct frequencies corresponding to the particular TM modes. For the first Brillouin zone ($-\pi < kz_0 < \pi$) of the dispersion relation, the values of the normalized wavenumber kz_0 which correspond to the seven resonant axial modes are $0\pi/6, \pi/6, 2\pi/6, 3\pi/6, 4\pi/6, 5\pi/6$, and $6\pi/6$, respectively. We will designate these axial modes by $TM_{0s}(N\pi/6)$ hereafter.

A. Electric Field Lines of the Fundamental Mode

Using the derived field equations in the SWS, the electric field lines are calculated. The method of computation is identical to that developed by Ogura *et al.* [18], with a modification for the higher order modes. Examples of the electric field patterns of the TM_{01} mode are depicted in Fig. 3(a) and (b), respectively, for $TM_{01}(0\pi/6)$ and $TM_{01}(6\pi/6)$ modes. The separations Δr between the field lines in the radial direction are so chosen that $E_z \Delta r$ =constant at the axial position $E_r = 0$. The density of the field lines in the radial direction represents the strength of the electric field qualitatively. For the $TM_{01}(0\pi/6)$ mode in Fig. 3(a), the electric field is fairly uniform in the axial direction, and the radial variation of the field has a maximum on the axis of the structure. The axial pattern of the fields has six zero points ($E_z = 0$) for the $TM_{01}(6\pi/6)$ modes as shown in Fig. 3(b). The periodic nature of the field lines depicted in Fig. 3(b) can be explained by the contribution of the Floquet harmonics for $n = 0$ to the resonant axial modes.

B. Field Patterns of Higher-Order Modes

The numerical calculation of the field patterns for the higher order modes $[TM_{0s}(s > 1)]$ is complicated. We followed

an improved technique from the case of the fundamental mode [18], and have tried to calculate the electric field lines for the TM_{02}, TM_{03}, and TM_{04} modes. Some of the results for the TM_{04} mode are presented in Fig. 4(a) and (b), respectively, for the case of $TM_{04}(0\pi/6)$ and $TM_{04}(6\pi/6)$ modes. The field patterns have fine and peculiar structures and differ considerably from those of the TM_{01} mode in Fig. 3. The radial distribution of the electric field lines in Fig. 4 is localized and separated into two parts: the peripheral and the central axis regions. The possible explanations for this difference can be given by the contribution of the Floquet harmonics involved in the SWS. This will be discussed in detail in the following subsection.

C. Floquet Harmonics of the Electromagnetic Fields in the Structure

The number of Floquet harmonics to represent the EM fields are practically limited by the computation time and the relative magnitude of the amplitude factor A_n's. The values of A_n differ from mode to mode as shown in Fig. 5(a) and (b), respectively, for TM_{01} and TM_{04} modes. In general, A_n decreases with increasing $|n|$, namely, A_0 within the first Brillouin zone of the dispersion relation is the largest. In Fig. 5(a), at $kz_0 = 0$, the relation between A_n's becomes $|A_n| = |A_{-n}|$ and $|A_n| \approx |A_{-n-1}|$ at $kz_0 = \pi$. At $r = 0$, the nonzero field component is E_z, and it is proportional to $A_0 + A_{-1}\exp[-i(2\pi/z_0)z] + A_1\exp[i(2\pi/z_0)z] + \cdots$. As shown in Fig. 5(a), the contribution of the $n = 0$ Floquet harmonic to E_z is predominant, and the amplitudes of the higher order harmonics are very small except at $kz_0 \approx \pi$ for the $TM_{01}(6\pi/6)$ mode. For this reason, the field lines of the $TM_{01}(0\pi/6)$ mode, as shown in Fig. 3(a), are almost straight lines for $r \leq R_0$. On the other hand, the field lines of the $TM_{01}(6\pi/6)$ mode are determined by the $n = 0$ and $n = -1$ Floquet harmonics. These two harmonics have the same field variations in the z-direction with a period of $2z_0$ and, hence, we obtain the field pattern with the periodicity depicted in Fig. 3(b).

For the TM_{04} mode in Fig. 5(b), the values of $A_{\pm 1}$ become greater than A_0 for small values of k within the first Brillouin zone of the dispersion curve. This result is novel and was not known in the previous works [14]–[16], [18]. The effects of this unusual behavior are observed in the electric field patterns of the structure shown in Fig. 4. In Fig. 5(b), as k increases, $|A_n|$ approaches $|A_{-n-1}|$ at $kz_0 = \pi$, as is observed for the TM_{01} mode in Fig. 5(a). The field quantities of the $TM_{04}(0\pi/6)$ mode in Fig. 5(b) are nearly proportional to $A_{-1}\exp[-i(2\pi/z_0)z] + A_1\exp[i(2\pi/z_0)z]$, which is periodic with period z_0. This fact can be seen from the field patterns of the $TM_{04}(0\pi/6)$ mode as shown in Fig. 4(a). As kz_0 approaches π, the field patterns of the $TM_{04}(6\pi/6)$ mode near $r = 0$ as shown in Fig. 4(b), have a periodicity $2z_0$, which is similar to that for the $TM_{01}(6\pi/6)$ mode in Fig. 3(b).

The harmonic components of $E_z(r = 0, z)$ are shown in Fig. 6(a) and (b) for the TM_{01} mode and in Fig. 6(c) and (d) for the TM_{04} mode. The EM fields are normalized by A_0. The thick, solid curves in the figures represent the total value

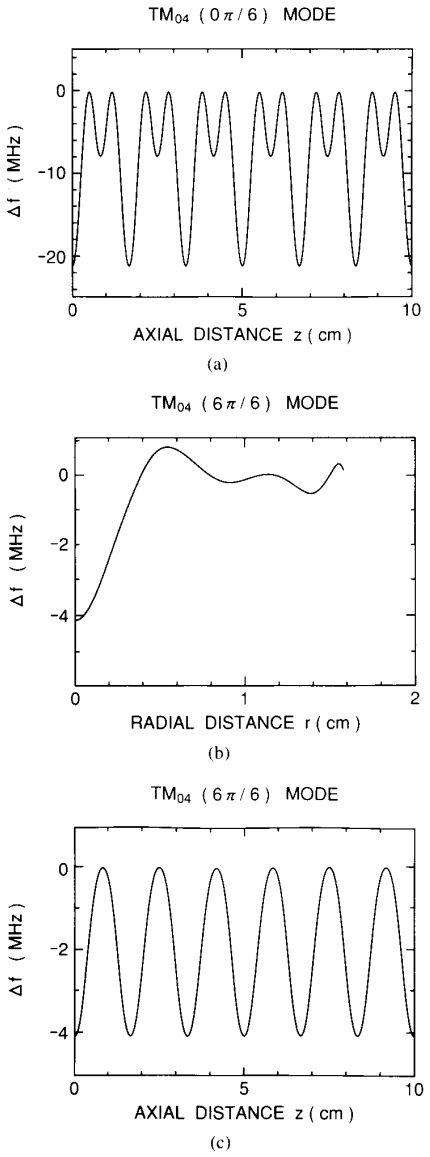

Fig. 7. Resonance frequency shift Δf of the axial resonant modes for the TM_{04} mode due to perturbation by a spherical metallic bead. (a) Axial changes in Δf of the $TM_{04}(0\pi/6)$ mode for the bead at $r = 0$; (b) radial changes in Δf of the $TM_{04}(6\pi/6)$ mode for the bead at $z = Nz_0$; (c) axial changes in Δf of the $TM_{04}(6\pi/6)$ mode for the bead at $r = 0$. Here, $N = 1, 2, \cdots, 6$.

of E_z. The thin, dashed and chained curves in Fig. 6 express E_z components at $r = 0$ denoted by the harmonic number n in (1), which can be understood if one compares to the values of A_n at $kz_0 = 0$ and $kz_0 = \pi$ in Fig. 5(a) and (b). The amplitudes of the higher order harmonics not expressed are very small compared to those shown in Fig. 6. The z-direction periodicities of E_z—as depicted in Fig. 6(a)–(d)—correspond, respectively, to those of Figs. 3(a) and (b), and 4(a) and (b). In Fig. 6(a), the contribution of the $n = \pm 1$ harmonics to E_z results in a small superimposed perturbation in the z-direction.

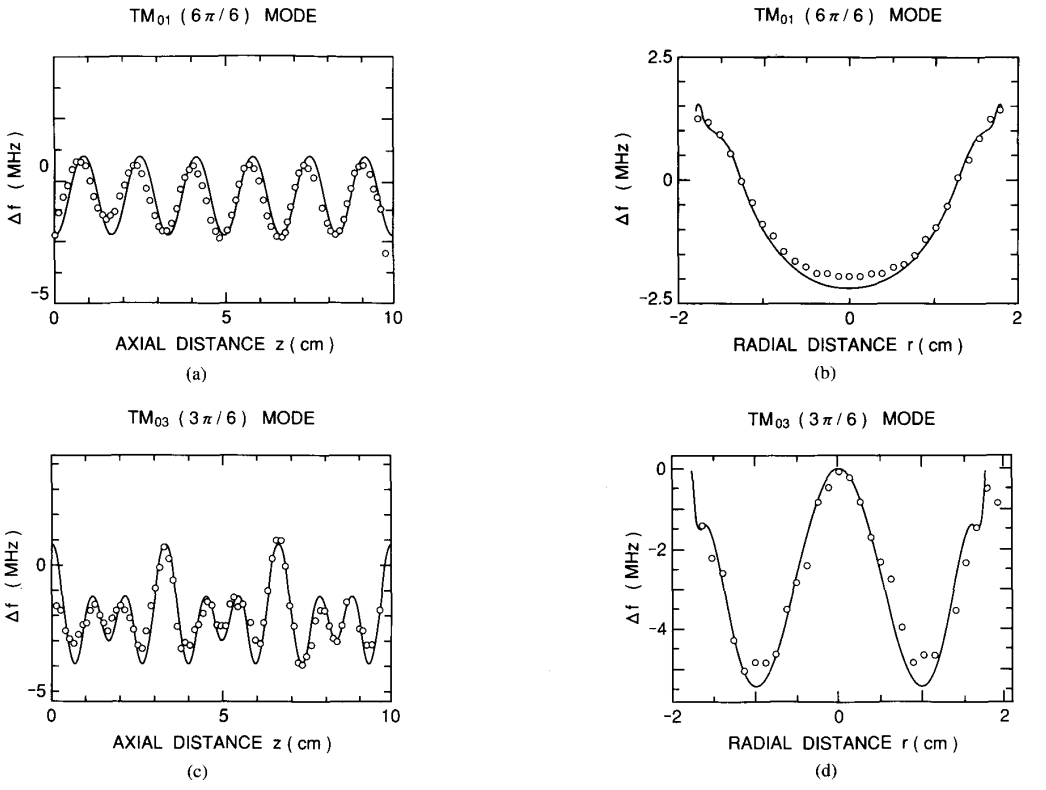

Fig. 8. Comparison of numerical and experimental results of frequency shift Δf by the displaced bead in axial and radial directions. The solid curves indicate the numerical results, and the open circles represent the corresponding experimental results. The axial data were measured by the bead at a radial position $r = 0.543$ cm. (a) Axial changes in Δf for the $TM_{01}(6\pi/6)$ mode; (b) radial changes in Δf for the $TM_{01}(6\pi/6)$ mode; (c) axial changes in Δf for the $TM_{03}(3\pi/6)$ mode; (d) radial changes in Δf for the $TM_{03}(3\pi/6)$ mode.

The effect of this perturbation can easily be observed in the field lines for the $TM_{01}(0\pi/6)$ mode in Fig. 3(a).

The above results for the TM_{04} mode are never trivial and have not been clarified in the past in the literature [14]–[18]. In usual cases, the fundamental A_0 term is dominant in (1) as shown in Fig. 6(b) and (d); the shortest axial period of E_z is $2z_0$ for $kz_0 = \pi$, as was shown by Fig. 3(b) and Fig. 4(b). On the other hand, in the special case where $|A_{\pm 1}|$ is larger than A_0, as shown in Fig. 5(b), the axial period can become as small as z_0 for $kz_0 \approx 0$, which is much shorter than the usual minimum period of $2z_0$.

IV. Perturbation Technique

The perturbation technique is a powerful method to measure EM field variations inside the resonant cavity [19]. This technique has been employed in the following analysis of SWS cavity, and the numerical results have been compared to experimental ones obtained at the University of Maryland [20].

When there exists a small metallic sphere bead with radius r_0 in the cavity, the EM fields in the cavity are perturbed and the resonance frequency of the cavity changes by an amount of Δf. If the perturbation is small enough, Δf can be calculated approximately with the unperturbed field quantities E_z, E_r, and H_θ given by (6)–(8). The resultant expression for Δf becomes [19], [20]

$$\frac{\Delta f}{f_0} = \frac{\frac{4}{3}\pi r_0^3(\frac{3}{2}\mu_0|H_\theta|^2 - 3\epsilon_0(|E_z|^2 + |E_r|^2))}{\int_V(\mu_0|H_\theta|^2 + \epsilon_0(|E_z|^2 + |E_r|^2)\,dV)}. \quad (9)$$

From (9), the field quantities are closely related to the frequency shift of the SWS cavity due to the bead. In the case of a spherical bead, the EM field quantities cannot be determined separately, because an unidirectional perturbation is impossible to achieve with the spherical bead perturber. The perturbation in E is always accompanied by a perturbation in H.

The calculated values of the frequency shift Δf for the TM_{04} mode, with a bead radius of 0.1195 cm, are presented in Fig. 7. The axial changes in Δf in Fig. 7 are calculated with the perturber at $r = 0$. The axial changes in Δf for the $TM_{04}(0\pi/6)$ mode are shown in Fig. 7(a). The radial and axial changes in Δf for the $TM_{04}(6\pi/6)$ mode are shown in Fig. 7(b) and (c), respectively. At $r = 0$, $E_r = H_\theta = 0$ and the only nonzero field component in (9) is E_z, and, hence, Δf in the axial direction as shown in Fig. 7(a) and (c), respectively, for $TM_{04}(0\pi/6)$ and $TM_{04}(6\pi/6)$ modes are directly proportional to $-|E_z|^2$. In other words, the results presented in Fig. 7(a) and (c) are proportional to the square of the axial profiles of total E_z in Fig. 6(c) and (d). Hence, at $r = 0$, we can obtain the quantitative information about

the axial electric field in the SWS from the Δf data. It should be noted that the solid curve in Fig. 6(c) is not symmetric regarding E_z ($r = 0$)$= 0$. The curve in Fig. 7(a) is therefore not simply sinusoidal. For $r \neq 0$, however, using the spherical perturber, it is impossible to measure quantitatively the individual fields involved in Δf. The radial variations of Δf are dependent on E_z, E_r, and H_θ. In the case of $r \neq 0$, at the axial positions where $E_r = 0$, both contributions from E_z and H_θ to Δf cannot be ignored as is seen from (9). The positive region in the radial profile of Δf for the $TM_{04}(6\pi/6)$ mode, in Fig. 7(b), is ascribed to H_θ. The axial variations of Δf for the $TM_{04}(0\pi/6)$ mode, in Fig. 7(a), are very rapid compared to those for the $TM_{01}(6\pi/6)$ mode, as shown in Fig. 8(a) by the solid curve. Experimentally, it is difficult to measure axial changes in Δf for the $TM_{04}(0\pi/6)$ mode, in Fig. 7(a), because of the very rapid variation of the fields in the axial direction. However, the $TM_{04}(6\pi/6)$ mode in Fig. 7(c) has variations of Δf similar to those observed for the $TM_{01}(6\pi/6)$ mode in Fig. 8(a). These modes have field variations which are not very rapid in the axial direction as depicted in Fig. 6(b) and (d). The numerical results of Δf have been compared to experimental measurements [20], and some of these results are shown in Fig. 8. The axial and radial changes in Δf for the $TM_{01}(6\pi/6)$ mode are shown in Fig. 8(a) and (b), respectively. The axial and radial changes in Δf for the $TM_{03}(3\pi/6)$ mode are shown in Fig. 8(c) and (d), respectively. The open circles represent the experimental data, and the solid curves are the present numerical results. The numerical data presented in Fig. 8(a) and 8(c) are for the bead at a radial position $r = 0.543$ cm from the axis. By comparing the frequency shift to the field profiles, one can determine the axial resonant modes in the SWS to be $TM_{01}(6\pi/6)$ and $TM_{03}(3\pi/6)$ modes. The agreement between the numerical and experimental results can be clearly estimated from the figures. The discrepancy between them lies within the range of 10–20%.

V. Discussion and Conclusion

We have numerically analyzed the EM quantities of fundamental and higher order axial TM modes in a finite length SWS. It is found that, for the higher order modes, the amplitudes of the Floquet harmonics show unusual behavior as depicted in Fig. 5(b) for the TM_{04} mode. For the $TM_{04}(0\pi/6)$ mode ($kz_0 = 0$), the field quantities are mainly determined by the Floquet harmonics with $n = -1$ and 1, and the fields have an unusual short period of z_0 as shown in Figs. 4(a) and 6(c). This indicates that the period of field modulations can decrease to z_0, which is small compared to that for the usual modes in cylindrical waveguides where the period is larger than $2z_0$. Such a mode with short field modulations may become important for higher frequency operation of BWO's.

The numerical results presented in this paper are being verified experimentally at the University of Maryland [20]. Generally speaking, it is impossible to reconstruct the field distributions including phase change by the frequency shift measurements only, because the frequency shift is related to only the absolute values of the EM fields, as is seen from (9). In some cases, however, the experimental results can be compared to the numerical calculations as shown in Fig. 8. It is concluded that the measured resonant modes are $TM_{01}(6\pi/6)$ in Fig. 8(a) and (b), and $TM_{03}(3\pi/6)$ in Fig. 8(c) and (d). The agreement between the numerical and experimental data is quite satisfactory.

To determine the dispersion characteristics of an SWS cavity, shorted plates are placed at both ends and the resonant modes are excited by a suitable mode launcher at one of the end plates. The degree of coupling between the mode launcher and the SWS determines the type of mode launcher to be used in the experiment. If the coupling between the mode launcher and the cavity is strong, complete reflection on the input antenna side cannot be expected. For a disc-type mode launcher, the reflection coefficient at the input end will be small, and consequently our assumption of perfectly shorted ends of the SWS becomes inapplicable. Hence, we prefer a short wire antenna at the center of the plate as a mode launcher to excite the cavity. However, it is difficult to excite the surface wave modes near $kz_0 = \pi$, as was reported in [20].

References

[1] V. L. Granatstein and I. Alexeff, *High-Power Microwave Sources*. Boston, MA: Artech House, 1987.

[2] R. A. Kehs, A. Bromborsky, B. G. Ruth, S. E. Graybill, W. W. Destler, Y. Carmel, and M. C. Chang, "A high power backward wave oscillator driven by a relativistic electron beam," *IEEE Trans. Plasma Sci.*, vol. PS-13, pp. 559–562, Dec. 1985.

[3] Y. Carmel, K. Minami, R. A. Kehs, W. W. Destler, V. L. Granatstein, D. K. Abe, and W. L. Lou, "Demonstration of efficiency enhancement in a high power backward wave oscillator by plasma injection," *Phys. Rev. Lett.*, vol. 62, pp. 2389–2392, May 1989.

[4] J. A. Swegle, R. A. Anderson, J. F. Camacho, B. R. Poole, M. A. Rhodes, E. T. Rosenbury, and D. L. Shaeffer, "Scaling studies and time-resolved microwave measurements on a relativistic backward-wave oscillator," *IEEE Trans. Plasma Sci.*, vol. 21, pp. 714–724, Dec. 1993.

[5] X. Zhai, E. Garate, R. Prohaska, G. Benford, and A. Fisher, "Experimental Study of a plasma-filled backward wave oscillator," *IEEE Trans. Plasma Sci.*, vol. 21, pp. 142–150, Feb. 1993.

[6] D. K. Abe, "Experimental studies of overmoded high power microwave generators," Ph.D. dissertation, Univ. of Maryland, 1992 (unpublished).

[7] S. P. Bugaev *et al.*, "Investigation of millimeter wavelength range relativistic diffraction generator," *IEEE Trans. Plasma Sci.*, vol. 18, pp. 518–524, June 1990.

[8] ——, "Relativistic multiwave Cerenkov generators," *IEEE Trans. Plasma Sci.*, vol. 18, pp. 525–536, June 1990.

[9] K. Halbach and R. F. Holsinger, "SUPERFISH—A computer program for evaluation of RF cavities with cylindrical symmetry," *Particle Accelerator*, vol. 7, pp. 213–222, 1976.

[10] U. Van Rienen and T. Weiland, "Triangular discretization method for the evaluation of rf fields in waveguides and cylindrically symmetric cavities," *Particle Accelerators*, vol. 20, pp. 239–265, 1987.

[11] R. K. Cooper and M. E. Jones, "The physics of codes," in *High-Brightness Accelerators*, A. K. Hyder, M. F. Rose, and A. H. Guenter, Eds. New York: Plenum, 1988, pp. 233–255.

[12] A. Bromborsky and B. Ruth, "Calculation of TM_{0n} dispersion relations in a corrugated cylindrical waveguides," *IEEE Trans. Microwave Theory Tech.*, vol. MTT-32, pp. 600–605, June 1984.

[13] J. A. Swegle *et al.*, "Backward wave oscillators with rippled wall resonator," *Phys. Fluids*, vol. 28, pp. 2882–2894, 1985.

[14] K. Minami *et al.*, "Linear theory of electromagnetic wave generation in a plasma-loaded corrugated-wall resonator," *IEEE Trans. Plasma Sci.*, vol. 18, pp. 537–545, June 1990.

[15] M. M. Ali *et al.*, "Linear analysis of a localized plasma loaded backward wave oscillator driven by an annular intense relativistic electron beam," *J. Phys. Soc. Japan*, vol. 60, pp. 2655–2664, Aug. 1991.

[16] M. M. Ali, K. Ogura, K. Minami, T. Watanabe, W. W. Destler, and V. L. Granatstein, "Linear analysis of a plasma-filled backward wave oscillator," *Phys. Fluids*, vol. B4, pp. 1023–1032, Apr. 1992.

[17] R. Sawhney, K. P. Maheshwari, and Y. Choyal, "Effect of plasma on efficiency enhancement in a high-power relativistic backward wave oscillator," *IEEE Trans. Plasma Sci.*, vol. 21, pp. 609–613, Dec. 1993.
[18] K. Ogura, K. Minami, M. M. Ali, K. Kan, T. Nomura, Y. Aiba, A. Sugawara, and T. Watanabe, "Analysis of field lines and Poynting vectors in corrugated wall waveguides," *J. Phys. Soc. Japan*, vol. 61, pp. 3966–3975, Nov. 1992.
[19] L. C. Maier, Jr., and J. C. Slater, "Field strength measurement in resonant cavities," *J. Appl. Phys.*, vol. 23, pp. 68–77, Jan. 1952.
[20] W. Main, Y. Carmel, K. Ogura, J. Weaver, G. S. Nusinovich, J. P. Tate, J. Rodgers, A. Bromborsky, S. Watanabe, M. R. Amin, K. Minami, W. W. Destler, and V. L. Granatstein, "The electromagnetic properties of open and closed overmoded slow wave resonators for interaction with relativistic electron beams," *IEEE Trans. Plasma Sci.*, vol. 22, no. 2, pp. 566-577, Oct. 1994.

Md. Ruhul Amin was born in Rangpur, Bangladesh, in 1959. He received the B.Sc. (EEE) degree from the University of Rajshahi in 1984, and the M.Sc. (EEE) degree from Bangladesh University of Engineering and Technology, Dhaka, Bangladesh, in 1987.

He is now on sabbatical from Bangladesh Institute of Technology, Rajshahi, where he is an assistant professor in the Electrical and Electronic Engineering Department. He is presently working toward the Ph.D. degree at the Graduate School of Science and Technology, Niigata University, Japan. His research interests include theoretical and experimental investigations of high-power microwave devices, and semiconductor power electronic drives.

Mr. Amin is a member of the Institution of Engineers Bangladesh (IEB) and the Physical Society of Japan.

K. Ogura, photograph and biography not available at time of publication.

H. Kitamura, photograph and biography not available at time of publication.

K. Minami, photograph and biography not available at time of publication.

T. Watanabe, photograph and biography not available at time of publication.

Y. Carmel, (S'66–M'69–S'71–M'74–SM'90) photograph and biography not available at time of publication.

W. Main, (M'93) photograph and biography not available at time of publication.

J. Weaver, photograph and biography not available at time of publication.

W. W. Destler, (M'84–SM'90–F'92) photograph and biography not available at time of publication.

V. L. Granatstein, (S'59–M'64–M'84–SM'86–F'92) photograph and biography not available at time of publication.